Published in final edited form as:
Invest Ophthalmol Vis Sci. 2007 October ; 48(10): 4597–4607. doi:10.1167/iovs.07-0349.

3D Histomorphometry of the Normal and Early Glaucomatous Monkey Optic Nerve Head: Lamina Cribrosa and Peripapillary Scleral Position and Thickness

Hongli Yang[*,2], **J. Crawford Downs, PhD**[*,1,2], **Christopher Girkin, MD**[3], **Lisandro Sakata, MD**[4], **Anthony Bellezza, PhD**[5], **Hilary Thompson, PhD**[6], and **Claude F. Burgoyne, MD**[1,2]

[1]Devers Eye Institute, Legacy Health System, Portland Oregon

[2]Department of Biomedical Engineering, Tulane University, New Orleans, Louisiana

[3]Department of Ophthalmology, University of Alabama, at Birmingham, Birmingham, Alabama

[4]Singapore Eye Research Institute (SERI), Singapore National Eye Center, Singapore

[5]Third Eye Associates, Camden, New Jersey

[6]School of Public Health, Louisiana State University Health Sciences Center, New Orleans, Louisiana

Abstract

Purpose—To three-dimensionally delineate the anterior and posterior surface of the lamina cribrosa, scleral flange and peripapillary sclera so as to determine the position and thickness of these structures within digital three-dimensional (3D) reconstructions of the monkey optic nerve head (ONH).

Methods—The trephinated ONH and peripapillary sclera from both eyes of three early glaucoma (EG) monkeys (one eye Normal, one eye given laser-induced EG) were serial-sectioned at 3-μm thickness, with the embedded tissue block face stained and imaged after each cut. Images were aligned and stacked to create 3D reconstructions, within which Bruch's membrane opening (BMO) and the anterior and posterior surfaces of the lamina cribrosa and peripapillary sclera were delineated in 40 serial, radial (4.5° interval), digital, sagittal sections. For each eye, a BMO zero reference plane was fit to the 80 BMO points, which served as the reference from which all position measurements were made. Regional laminar, scleral flange, and peripapillary scleral position and thickness were compared between the Normal and EG eyes of each monkey and between treatment groups by analysis of variance.

Results—Laminar thickness varies substantially within the Normal eyes and is profoundly thicker within the three EG eyes. Laminar position is permanently posteriorly deformed in all three EG eyes, with substantial differences in the magnitude and extent of deformation among them. Scleral flange and peripapillary scleral thickness vary regionally within each Normal ONH with the scleral flange and peripapillary sclera thinnest nasally. Overall, the scleral flange and peripapillary sclera immediately surrounding the ONH are posteriorly displaced relative to the more peripheral sclera.

Conclusion—Profound fixed posterior deformation and thickening of the lamina is accompanied by mild posterior deformation and thinning of the scleral flange and peripapillary sclera at the onset

Reprint requests: Claude F. Burgoyne, MD, Optic Nerve Head Research Laboratory, Devers Eye Institute, 1225 NE 2nd Ave, PO Box 3950, Portland OR 97208-3950. Email: cfburgoyne@deverseye.org.

[*]Ms. Yang and Dr. Downs share first authorship of this work.

of confocal scanning laser tomography detected (CSLT) ONH surface change in young adult monkey eyes with early experimental glaucoma.

Keywords

glaucoma; neural canal; optic nerve head; intraocular pressure; histomorphometry; sclera; lamina cribrosa; scleral flange

We have previously proposed that intraocular pressure (IOP) related optic nerve head (ONH) connective tissue damage is a defining feature of glaucomatous cupping[1]. We have additionally demonstrated permanent deformation of the ONH connective tissues within serial histologic sections[2] and two-dimensionally delineated, digital, three-dimensional (3D) reconstructions of monkey ONHs with early experimental glaucoma (EG)[3]. In both the histologic[2] and 3D reconstruction studies[3], posterior deformation and thickening of the lamina cribrosa was present within the EG monkey ONHs.

The current report is the second in a series of five articles devoted to 3D histomorphometric quantification of the ONH and peripapillary neural and connective tissues. In the first report[4], we introduced our method for 3D delineation of 13 ONH and peripapillary scleral landmarks, tested the method's reproducibility, and used it to describe enlargement and elongation of the neural canal within the EG eyes of three monkeys. In the current report, we concentrate on the position and thickness of the lamina cribrosa, scleral flange and peripapillary sclera so as to characterize the regional pattern of laminar and peripapillary scleral deformation and thickness alterations at the onset of CSLT-detected ONH surface change in these same three EG eyes.

A series of reports have demonstrated the efficacy of CSLT characterization of ONH surface change in detecting the onset and progression of ONH damage in ocular hypertension[5-7] We propose that the onset of CSLT-detected ONH surface change in an ocular hypertensive monkey or human eye is a manifestation of subsurface phenomena which include deformation and thickness changes of the prelaminar neural tissues, lamina cribrosa, and the peripapillary sclera. These phenomena are direct manifestations of neural and connective tissue pathophysiology that likely precede surface change and/or axonal insult.

In the current study, three monkeys were given moderate, laser-induced IOP elevations in one eye and sacrificed at the onset of CSLT-detected ONH surface change[2, 3] by perfusion fixation with both eyes set to an IOP of 10 mm Hg by anterior chamber manometer. Both ONHs of each animal were then 3D reconstructed and evidence for permanent subsurface, structural change within the EG ONH of each animal was sought within 3D histomorphometric characterizations of lamina cribrosa, scleral flange and peripapillary scleral position and thickness.

Our study was designed to detect permanent connective tissue deformation by perfusion fixation with IOP set to 10 mm Hg bilaterally for a 30-minute period of equilibration prior to death. Detecting permanent deformation of the connective tissues of the lamina cribrosa, scleral flange, and peripapillary sclera in EG is important because it provides evidence that these tissues are damaged early in the neuropathy. In addition, because these forms of subsurface structural change may precede clinically identifiable axonal insult, they may one-day be detectable by next- generation clinical imaging devices[8-16] and used to detect the onset of glaucomatous damage prior to visual field loss.

Three-dimensionally quantifying these deformations is important because it allows us to construct and refine finite element models of IOP-related neural and connective tissue stress and strain within these same ONHs[17-20]. Determination of the structural factors that influence

ONH biomechanical behavior should allow us to determine those factors that contribute most to individual susceptibility to glaucoma, and how remodeling of the ONH connective tissues in early glaucoma effects the biomechanical behavior of these tissues.

Materals and Methods

Animals

All animals were treated in accordance with The Association for Research in Vision and Ophthalmology (ARVO) Resolution on the Use of Animals in Ophthalmic and Vision Research. Three male cynomolgous monkeys, approximately 8 years of age, were used for these studies (see Table 1 of our previous report[3]).

ONH Surface Compliance Testing and Early Glaucoma

We have previously described our Laser Diagnostic Technologies (LDT, San Diego, CA) Confocal Scanning Laser Tomographic (CSLT)-based ONH surface compliance testing strategy[3, 21]. Briefly, both eyes of each monkey were imaged on three separate occasions while normal, then lasering of the trabecular meshwork was begun in one eye of each animal to elevate IOP. CSLT imaging was continued at 2-week intervals until the onset of significant permanent posterior deformation of the ONH surface in the lasered eye. See Table 1 and Figure 1 in our previous publication regarding the magnitude and duration of IOP elevation experienced by each animal[3]. Monkeys 2 and 3 were sacrificed three weeks and Monkey 1 six weeks after CSLT detection of ONH surface change. In Monkeys 1 and 2, IOP elevations were moderate with only one measurement higher than 30 mm Hg. In Monkey 3 elevated IOP was not detected[3].

Monkey Sacrifice and Perfusion Fixation at Prescribed IOP

For each monkey, both eyes were cannulated with a 27-gauge needle under deep pentobarbital anesthesia, and the IOP was set to 10 mm Hg using an adjustable saline reservoir. After a minimum of 30 minutes, the monkey was perfusion fixed via the descending aorta with 1 L of 4% buffered hypertonic paraformaldehyde solution followed by 6 L of 5% buffered hypertonic glutaraldehyde solution[4]. Following perfusion fixation, IOP was maintained for 1 hour, after which each eye was enucleated, all extraorbital tissues were removed, and the anterior chamber was removed 2 to 3 mm posterior to the limbus. By gross inspection, perfusion was excellent for all six eyes. The posterior scleral shells with intact ONH, choroid and retina were placed in 5% glutaraldehyde solution for storage.

Generation of the Aligned Serial Section Images for Each ONH and 3D ONH Reconstruction

These steps have been described in detail within our previous reports[3, 4]. Briefly, the ONH and peripapillary sclera were trephinated (6-mm diameter), pierced with alignment sutures, embedded in paraffin and mounted to a microtome. Then the block surface was stained with a 1:1 (v/v) mixture of Ponceau S and acid fuchsin stains, and imaged at a resolution of 2.5 × 2.5 μm per pixel. The sections were serially cut away at 3.0-μm-thickness, and the staining and imaging process was repeated after each cut. Imaging began at the vitreoretinal interface and continued approximately 200 μm into the retrolaminar orbital optic nerve. Serial section images were aligned in the anterior-to-posterior direction and stacked at 3.0-μm intervals into a 3D reconstruction of the ONH and peripapillary scleral connective tissues, which consist of approximately 1080 × 1520 × 400 voxels, each 2.5 × 2.5 × 3.0 μm in size.

3D Delineation of ONH and Peripapillary Scleral Landmark Points

Our 3D delineation technique has been described in detail in our previous report[4]. Briefly, using custom software based on the Visualization Toolkit (VTK, Clifton Park, NY), the 3D

ONH reconstruction is loaded into memory on a remote Linux server. The delineator assigns the approximate center of the neural canal as that reconstruction's center of rotation, around which 40, 7-voxel-thick, digital, radial, sagittal slices of the digital 3D reconstruction are serially served at 4.5° intervals to the delineator's workstation (Figure 1).

Within each digital section (Figure 1C), the delineator marks 7 landmark surfaces and 6 pairs of neural canal landmark points (one point on each side of the canal) (Figure 1D). In this report, only the anterior and posterior surfaces of the peripapillary sclera and lamina cribrosa, the neural canal wall and the neural canal landmark points (Figures 1B) are used.

While marking in the sagittal section view window (Figure 1D), the delineator is simultaneously viewing an adjacent window showing the cursor's 3D location within a digital transverse section image (Figure 1E) slaved to the sagittal section view. The delineator also can scroll through the adjacent six 1-voxel-thick sagittal section images to locate a section in which the landmark can be clearly identified. The 3D Cartesian coordinates and category for each mark are saved, generating a 3D point cloud that represents each of the marked structures (Figure 1F).

Clinical Alignment of the 3D Reconstruction

A high-resolution reconstruction of the central retinal vessels and the neural canal landmark points[4] is constructed and three-dimensionally overlaid onto a clinical fundus photo or CSLT image to accurately align the 3D marks to anatomic orientation (superior, inferior, nasal and temporal – see Figure 2 of our previous publication[4]).

BMO Zero Reference Plane

For each 3D ONH reconstruction, a least-squares ellipse is fit to the 80 marks defining BMO, creating a BMO zero reference plane (Figure 2B). All measurements of anterior laminar and peripapillary scleral position are made relative to this plane[4].

Lamina Cribrosa Position and Thickness

The definition and extent of the lamina cribrosa, scleral flange, and peripapillary sclera as structures are diagrammed and explained in Figure 2). Independent measures of laminar position and thickness are made at each delineated anterior laminar surface point. At each point, anterior laminar position is calculated as the distance from BMO zero reference plane (Figure 2C) along a vector normal to that plane. To determine laminar thickness, the anterior and posterior laminar surface points are fit to continuous anterior and posterior surfaces using a thin-plate B-spline (MATLAB, The Mathworks, Natick, MA). The smoothed anterior laminar B-spline surface is used to generate a normal vector at each delineated point (Figures 2D, 2E). Thickness of the lamina is calculated along each delineated point's normal vector as the shortest distance to the posterior laminar surface (Figure 2F).

Scleral Flange Position and Thickness

Scleral flange (defined in Figure 2B) position is determined at each delineated anterior surface point as described for the lamina. Due to it's unique geometry, scleral flange thickness is defined as the distance from the anterior scleral flange surface to the neural canal boundary surface, measured at each delineated anterior surface point along a vector parallel to the PSCO normal vector (Figures 2G, 2H).

Peripapillary Scleral Position and Thickness

Peripapillary scleral position and thickness are calculated at each delineated anterior scleral surface point as described for the lamina cribrosa.

Continuous Plots of Laminar, Scleral Flange, and Peripapillary Scleral Position and Thickness; Intra-animal Difference Map Generation

Continuous plots of position and thickness are generated for each eye by interpolating between the values measured at each delineated anterior surface point (Delaunay-based cubic interpolation; MATLAB). Data for the left eye is converted to right eye configuration for direct comparison (Figures 3, 4). Difference maps for each animal are generated by overlaying the BMO centroid for each eye and subtracting the Normal data from the EG eye data (Figures 3, 4).

Parameter Regionalization

To perform statistical inference testing, position and thickness data at each delineated point on the anterior surface were pooled into laminar, scleral flange, and peripapillary scleral structures as shown in Figure 5, top. Within the lamina cribrosa, position and thickness data at each delineated point is assigned to one of 17 sub-regions as depicted in Figure 5, top left. Scleral flange and peripapillary scleral position data were pooled together because they were identically obtained and assigned to one of 8 sub-regions as depicted in Figure 5, top right. Scleral flange and peripapillary scleral data thickness data were considered separately because their thicknesses were measured differently (see below) but were assigned to the same 8 sub-regions as depicted in Figure 5.

Inter-delineator Variability and Intra-delineator Reproducibility

Inter-delineator variability was assessed within data for all five delineators, in which they delineated both eyes of all three monkeys. Intra-delineator reproducibility was assessed within data for two of the five delineators, in which they delineated both eyes of Monkey 3 two additional times at least two weeks apart. The effect of delineator (overall and within each monkey) and delineation day were assessed within separate factorial analyses of variance (ANOVA).

Statistical Analyses

Factorial ANOVAs were used to assess the effects of delineator, region, and treatment group (Normal or EG) on the parameters lamina cribrosa position, lamina cribrosa thickness, scleral flange and peripapillary scleral position, scleral flange thickness and peripapillary scleral thickness, both by treatment group and between the two eyes of each monkey.

Results

Continuous Position Maps

Continuous maps of laminar, scleral flange and peripapillary scleral position relative to BMO zero reference plane are presented for each eye and for the difference between the EG and Normal eye of each monkey in Figure 3. It should be noted that in this description, and throughout this report, we use the histologic terms “anterior” and “posterior” to mean “inward” and “outward” movement of these structures relative to the vitreous cavity as detected by clinical examination.

Continuous maps of the differences in laminar, scleral flange, and peripapillary scleral position between the EG and Normal eyes of each monkey are presented in Figure 3. Laminar position is very similar in the 3 Normal monkey eyes, but the lamina is profoundly posteriorly displaced in all 3 EG eyes. The lamina is most posteriorly displaced centrally in all 3 EG eyes, with substantial extension of the posterior displacement into the infero-nasal region in Monkeys 1 and 3. Scleral flange and peripapillary scleral position relative to BMO zero reference plane in the 3 EG eyes is anterior compared to its position in the contralateral normal eyes, which is

the likely result of overall posterior deformation of the scleral flange and peripapillary sclera in all 3 EG eyes. In Monkeys 1 and 2, there is additional posterior displacement of the nasal scleral flange and peripapillary sclera that suggests an additional component of tilt (nasal down, temporal up) in these two eyes.

Continuous Thickness Maps

Continuous maps of laminar, scleral flange and peripapillary scleral thickness are presented for both the Normal and EG eye of each monkey in Figure 4. Laminar thickness varies substantially among the three Normal eyes, being thinnest inferiorly and superiorly in Monkeys 1 and 3, and diffusely thicker in Monkey 2. The lamina is substantially thicker in all 3 EG eyes. The scleral flange and peripapillary sclera is thinnest immediately adjacent to the neural canal, particularly nasally, in both eyes of all three monkeys.

Continuous maps of the differences in laminar, and scleral flange and peripapillary scleral thickness between the EG and Normal eye of each monkey are shown in Figure 4. While the lamina is focally thinner within the superior and inferior regions of Monkey 2 and nasal and temporal regions of Monkey 3, the lamina is diffusely thicker within most regions of all 3 EG eyes. Both the scleral flange and peripapillary sclera are mildly thinner within the EG eyes of all 3 monkeys, with each EG eye demonstrating focal nasal and infero-nasal thickening of variable extent.

Overall Position and Thickness of the Lamina Cribrosa, Scleral Flange, and Peripapillary Sclera by Treatment and Delineator

Table 1 reports the Normal eye data and overall treatment difference of all five parameters for all five delineators. Overall, the lamina was more posterior (90 to 106 μm) and thicker (30 to 62 μm) and the scleral flange and peripapillary sclera was more anterior (16 to 44 μm) in the EG eyes relative to BMO within the data for all five delineators ($P<0.05$, ANOVA). Changes in scleral flange and peripapillary scleral thickness were of smaller magnitude and inconsistent direction and significance.

Overall Position and Thickness of the Lamina Cribrosa, Scleral Flange, and Peripapillary Sclera within Each Monkey

Table 2 reports the Normal eye data and overall treatment difference of all five parameters within each monkey for Delineator 1. Overall laminar position is significantly more posterior in all 3 EG eyes (79 to 118 μm). Overall the scleral flange and peripapillary sclera is significantly more anterior in 2 of the 3 EG eyes, with Monkey 2 demonstrating no significant overall difference. It should be noted that since the BMO zero reference plane is tethered to the scleral flange and moves in concert with it, the relative anterior position of the peripheral peripapillary sclera in the EG eyes (Figure 3) is the likely result of an overall posterior deformation of the ONH, scleral flange, and immediate peripapillary sclera in these eyes. Overall laminar thickness is significantly increased (23 to 61 μm) in the EG eyes of all 3 monkeys. Scleral flange thickness was not significantly different by treatment within any monkey, and peripapillary scleral thickness was only decreased within the EG eye of Monkey 2. These differences were similar within the data of all 5 delineators (data not shown).

Overall Regional Position and Thickness of the Lamina Cribrosa and Peripapillary Sclera by Treatment

The differences in regional position and thickness between the pooled Normal and EG eyes are presented for Delineator 1 in Figure 5. Overall, most regions of the lamina cribrosa are significantly more posterior (-36 to -163 μm) in the EG eyes, with the highest deformations in the central and inferior mid-peripheral regions ($P<0.05$, ANOVA). Overall, the scleral flange

and peripapillary sclera was significantly more anterior (15-60 μm) in the superior, supero-temporal, temporal, and infero-temporal sub-regions, and significantly more posterior in the supero-nasal and nasal sub-regions (-7 to -20 μm) in the EG eyes (P<0.05, ANOVA). Again, the relative anterior position of the peripheral peripapillary sclera in the EG eyes is the likely result of an overall posterior deformation of the ONH, scleral flange, and immediate peripapillary sclera in these eyes.

The lamina is significantly thicker (21 - 61 μm) in all but two of 17 sub-regions in the EG eyes (P<0.05, ANOVA), with the greatest thickness increases present in the inferior and infero-nasal quadrants. In contrast, the scleral flange demonstrated no significant differences in sub-regional thickness and the peripapillary sclera demonstrated significant thinning (up to 44 μm) in three of 16 regions in the EG eyes (P<0.05, ANOVA). The reported treatment effects were similar within the data from all 5 delineators (data not shown).

Regional Position and Thickness of the Lamina Cribrosa and Peripapillary Sclera by Treatment within each Monkey

Regional position and thickness differences between the Normal and EG eye of each monkey are presented for Delineator 1 in Figure 6. The lamina is significantly more posterior within all 3 EG eyes (-118 to -199 μm centrally), with the largest posterior deformations in the central, inferior, and infero-nasal sub-regions (P<0.05, ANOVA). The scleral flange and peripapillary sclera again measure more anterior relative to BMO reference plane within the temporal regions of each EG eye.

In general, the lamina was significantly thicker in all three EG eyes compared to their contralateral Normal controls, although the pattern and magnitude of glaucomatous thickening was different in each monkey (Figure 6; P<0.05, ANOVA). Lamina cribrosa thickness was significantly increased in Monkey 1, with the greatest changes seen superiorly and inferiorly. Lamina cribrosa thickness is increased nasally and temporally in the EG eye Monkey 2. The lamina is thickened more diffusely in the EG eye of Monkey 3, although the treatment effect is greatest inferiorly. There were no statistically significant regions of laminar thinning in any of the EG eyes. No statistically significant differences in scleral flange thickness were measured in any of the EG eyes. Statistically significant thinning of the peripheral peripapillary sclera is present in the EG eye of Monkey 2, but is only present within a single region of Monkeys 1 and 3.

Inter-delineator Variability

All five thickness and position parameters are presented for all five delineators in Table 1. While the effect of delineator was significant for position and thickness by treatment (P<0.001, ANOVA), all five delineators agreed in the direction and magnitude of glaucomatous change in all parameters except the thickness of the peripapillary sclera (Table 1). The effect of delineator was significant (P<0.001) for both position and thickness within all three monkeys considered individually, however, their effect compared to treatment was small for position and modest for thickness.

Intra-delineator Repeatability

All five thickness and position parameters are presented for two delineators marking both eyes of Monkey 3 on three different days in Table 3. The effect of delineation day was statistically significant for all parameters (P<0.05, ANOVA) except the thickness of the peripapillary scleral flange (P=0.31). However, the magnitude and direction of inter-eye differences between the two eyes of Monkey 3 are very similar within and between the three sessions of each delineator (Table 3).

Discussion

Accurately characterizing ONH and peripapillary scleral connective tissue architecture has been the goal of a large and important literature, which was extensively reviewed in two previous reports[2, 4, 8]. In a previous report, we introduced our method for high-resolution, digital, 3D reconstruction of the ONH tissues and used it to reconstruct the Normal and EG ONHs of three monkeys with early experimental glaucoma in one eye[3]. In the first article of this series[4], we introduced a new method for 3D delineation and 3D quantification of ONH and peripapillary scleral neural and connective tissue architecture and used the 3D-delineated point clouds to quantitatively characterize neural canal architecture changes in early experimental glaucoma within the same reconstructions.

In the present report, we utilize a subset of the 3D-delineated point clouds to generate continuous maps of lamina cribrosa, scleral flange and peripapillary scleral position and thickness within both the Normal and EG eye of each animal so as to characterize the principal inter- and intra-animal differences between the Normal and EG eyes.

Our method of delineation of laminar and peripapillary scleral surfaces and the subsequent measurements of thickness and position of those structures exhibit low inter- and intra-delineator variability (Tables 1 and 3). Generally, the absolute position and thickness values as well as the magnitude of the EG treatment effects, both overall and within each monkey, were similar among delineators. For all parameters, two delineators consistently measured similar magnitudes and detected similar treatment effects within delineation sessions performed in both eyes of one monkey on three different days. However, both inter-delineator variability and intra-delineator reproducibility was better for position than thickness. Two factors may contribute to this difference. First, the biological graduation from the lamina to the retrolaminar septa can be difficult to discern, which makes the posterior laminar surface more difficult to delineate than the anterior surface. Second, treatment differences in position were larger than thickness, and therefore easier to detect.

The principal findings of this report are as follows. First, lamina cribrosa thickness varies substantially within the three Normal eyes and is profoundly thicker in the EG eye of all three monkeys. Second, the lamina cribrosa is permanently posteriorly displaced in all three EG eyes. Although lamina cribrosa position relative to BMO zero reference plane is similar within the three Normal eyes, the magnitude and area of the posterior laminar deformation are very different between the EG eyes. Third, scleral flange architecture and peripapillary scleral thickness vary regionally within each normal ONH, with the flange being thinnest nasally due to the oblique path of the nerve though the sclera (Figure 7). Inter-animal differences in these anatomic features are substantial within Normal eyes, and are not profoundly changed in EG. Fourth, the scleral flange and immediate peripapillary sclera is posteriorly deformed overall and in 2 of the 3 EG eyes.

Our findings suggest that permanent posterior deformation and thickening of the lamina cribrosa, and posterior deformation of the scleral flange and immediate peripapillary sclera are present at the earliest detectable stage of glaucomatous damage in the young adult monkey eye. Since each animal had IOP lowered to 10 mm Hg in both eyes for at least 30 minutes prior to perfusion fixation, and in a previous study, only minimal levels of anterior ONH surface movement were detected even 45 minutes after IOP lowering in glaucoma eyes[22], these changes likely represent permanent, irreversible ONH and peripapillary scleral deformation.

The clinical variability of ONH and peripapillary scleral connective tissue thickness within normal eyes holds important implications for connective tissue and axonal susceptibility to glaucomatous damage. We have previously proposed that the central pathophysiology of glaucomatous cupping is primary or secondary damage to the ONH connective tissues, which

results in the associated permanent deformation reported here. From an engineering standpoint, ONH connective tissue susceptibility to damage and permanent deformation should be directly related to its structural stiffness, which is a combination of the structure's geometry (tissue volume and morphology) and material properties (tissue stiffness). If all other components of structural stiffness were equal in two eyes, eyes with thicker lamina and thicker sclera should be more resistant to deformation and mechanical damage. Structurally stiffer eyes should therefore demonstrate a shallower form of glaucomatous cupping if damage and deformation do occur.

However, because the mechanisms of IOP-related axonal insult are likely to be multifactorial[1, 23], the relationship between ONH connective tissue thickness and axonal susceptibility are likely to be complex. Since the principle insults to the axons within the lamina cribrosa have yet to be elucidated, the implications of differences in lamina cribrosa thickness are not certain. A thicker lamina should be of benefit in those regions in which axonal transport blockage occurs due to high translaminar tissue pressure gradients[24], as increased laminar thickness serves to expand the length of the axon over which the pressure difference between the vitreous cavity and CSF is dissipated.

Our finding of increased lamina cribrosa thickness within these three EG eyes confirms the histologic findings of our previous report[2] in a new group of EG monkey eyes and has important implications. A considerable literature reports compression of the lamina cribrosa within moderately and severely damaged glaucomatous eyes[25-27]. Interestingly, Quigley et al.[26] reported compression of the lamina cribrosa in scanning electron micrographs of trypsin-digested human cadaver eyes with an early (pre-Goldman visual field loss) stage of glaucomatous damage.

The increase in laminar thickness that we report could be the result of several factors that include axonal swelling that is secondary to axonal transport blockage within the laminar trabeculae, edema of the neural and/or connective tissues, and remodeling and/or synthesis of laminar connective tissue in response to IOP-related damage. Several studies have shown that both retrograde and orthograde axonal transport are compromised by increases in IOP of less than 1 week's duration, but the degree to which intra-laminar axonal swelling and/or edema could contribute to laminar thickening is unknown. We have built the ability to quantify the microarchitecture of the lamina cribrosa and will report the results in the fourth paper of this series. These data suggest a very substantial increase in the volume of lamina cribrosa connective tissue (total connective tissue voxels) in these same three EG eyes compared to their Normal controls. Molecular and biochemical characterizations of EG changes within the monkey lamina cribrosa are currently underway in our laboratory.

Early deformation of the lamina cribrosa in all three EG eyes are greatest centrally, with the areas of maximum deformation extending inferiorly and inferior-nasally in 2 of the 3 EG eyes. Laminar deformation was confined to the central region in Monkey 2, which had the highest detected IOP exposure and the most robust connective tissue architecture (thickest lamina, least oblique canal, thickest scleral flange and thickest peripapillary sclera). These results suggest that posterior deformation of the central lamina appears to be the earliest permanent deformation of these tissues in experimental EG.

In this report, we introduce the concept of the scleral flange as the transition zone between the lamina cribrosa and peripapillary sclera and suggest it should be treated as a unique component of the ONH connective tissue architecture. The scleral flange contains the penetrating branches of the Circle of Zinn-Haller and underlies important clinical landmarks and behaviors that are central to peripapillary scleral involvement in the neuropathy. Figure 7 illustrates scleral flange architecture within the Normal eyes of all three monkeys, and demonstrates the fundamental

relationship between neural canal and scleral flange obliqueness at any given BMO clock-hour location.

The peripapillary sclera has been shown to be the site of substantial stress and strain concentrations within initial finite element models of the human[18, 20] and monkey ONH[17]. To date, these models have not been detailed enough to incorporate scleral flange architecture into their estimates. Our results demonstrate that the scleral flange is susceptible to posterior deformation, which may significantly influence laminar deformation and strain. Regions of the flange that are thin or oblique should be most susceptible to posterior deformation.

Our overall findings suggest the following model for early permanent deformation of the ONH and peripapillary scleral connective tissues in monkey experimental glaucoma (Figure 8). First, the lamina cribrosa is thickened and posteriorly deformed, greatest centrally, with focal progression to the periphery (not shown). The scleral flange and peripapillary sclera are together displaced posteriorly. The outer aspect of the neural canal is diffusely expanded as a result of the posterior deformation of the peripapillary sclera, while the inner entrance to the neural canal is only focally expanded[4] (not shown).

The pattern of axonal loss in early human glaucoma has been traditionally ascribed to the superior and inferior poles of the ONH[28, 29]. However, in these three EG eyes, early laminar, scleral flange and peripapillary scleral deformations and thickness alterations are not consistently localized to the superior and inferior quadrants in the EG eyes (Figures 5 and 6). A definitive study co-localizing alterations in the ONH prelaminar neural tissue and lamina cribrosa with orbital optic nerve axonal loss in these three EG eyes will be the subject of a future report.

The limitations of our method of 3D reconstruction have previously been discussed[3, 4] and include: 1) anterior-to-posterior resolution is limited to 3 μm by the fact that the current stain penetrates approximately 2.5 μm into the embedded tissue block face; 2) the stain is applied manually to the block face, so staining variation between section images can be substantial; 3) there are tissue shrinkage effects (both from fixation and embedding) associated with this technique, but since all eyes were treated identically, comparisons between the two eyes of each monkey and within treatment groups should be valid; and 4) we have not yet characterized physiologic, inter-eye differences for these parameters.

In addition, while all future monkey eye reconstructions will be aligned to clinical photos, clinical alignment of the 3D reconstruction for these three monkeys was done to CSLT images which may not provide as clear an image of the clinical optic disc margin. However, in a subsequent alignment of both eyes of Monkey 3 to clinical photos (the only animal for which they were available)[4] no substantial shift in alignment over that achieved with CSLT images was required.

Continuum and micro finite element models of each eye, which are derived from the 3D landmark point-clouds described above, are currently under construction. These models will characterize the magnitude and distribution of IOP-related stress and strain within the connective tissues of each 3D-reconstructed ONH. This characterization will allow us to establish the relationships between IOP-related stress and strain, ONH anatomy, and the permanent EG connective tissue deformations reported herein. These relationships, once elucidated, will provide valuable insight into the biomechanical factors that contribute to individual ONH susceptibility to glaucomatous damage.

Finally, we propose that visualization of the laminar, scleral flange and peripapillary scleral landmarks described in this report should become an important goal of clinical glaucoma imaging. In assessing the susceptibility of an individual ONH to a given level of IOP, the 3D

architecture of these structures may be central to the estimation of ONH susceptibility and the clinical assignment of target IOP. In addition, clinically detectable deformation and thickness changes of these deep structures may precede surface-detected structural and functional change at all stages of the neuropathy, and serve as a marker for the development and progression of the disease.

Acknowledgments

The authors gratefully acknowledge Jonathon Grimm, Budd Hirons, Juan Reynaud, and Pris Zhou without whom the development and implementation of this methodology would not have been possible.

Supported in part by USPHS grants R01EY011610 (CFB), K23EY13959 (CAG), and P30EY002377 (HWT) (departmental core grant) from the National Eye Institute, National Institutes of Health, Bethesda, Maryland; a grant from the American Health Assistance Foundation, Rockville, Maryland (CFB); a grant from The Whitaker Foundation, Arlington, Virginia (CFB); a grant from the Eyesight Foundation of Alabama (CAG); a Career Development Award (CFB) and a Physician-Scientist award (CAG) from Research to Prevent Blindness, Inc., New York, New York; and a grant from the Sears Trust, Mexico, Missouri.

References

1. Burgoyne CF, Downs JC, Bellezza AJ, Suh JK, Hart RT. The optic nerve head as a biomechanical structure: a new paradigm for understanding the role of IOP-related stress and strain in the pathophysiology of glaucomatous optic nerve head damage. Prog Retin Eye Res 2005;24:39–73. [PubMed: 15555526]
2. Bellezza AJ, Rintalan CJ, Thompson HW, et al. Deformation of the lamina cribrosa and anterior scleral canal wall in early experimental glaucoma. Invest Ophthalmol Vis Sci 2003;44:623–637. [PubMed: 12556392]
3. Burgoyne CF, Downs JC, Bellezza AJ, Hart RT. Three-dimensional reconstruction of normal and early glaucoma monkey optic nerve head connective tissues. Invest Ophthalmol Vis Sci 2004;45:4388–4399. [PubMed: 15557447]
4. Downs JC, Yang H, Girkin C, et al. Three Dimensional Histomorphometry of the Normal and Early Glaucomatous Monkey Optic Nerve Head: Neural Canal and Subarachnoid Space Architecture. IOVS. 2007In Press
5. Chauhan BCP, McCormick TAB, Nicolela MTM, LeBlanc RPM. Optic Disc and Visual Field Changes in a Prospective Longitudinal Study of Patients with Glaucoma. Arch Ophthalmology 2001;119:1492–1499.
6. Tan JC, Hitchings RA. Approach for identifying glaucomatous optic nerve progression by scanning laser tomography. Invest Ophthalmol Vis Sci 2003;44:2621–2626. [PubMed: 12766065]
7. Strouthidis NG, Scott A, Peter NM, Garway-Heath DF. Optic disc and visual field progression in ocular hypertensive subjects: detection rates, specificity, and agreement. Invest Ophthalmol Vis Sci 2006;47:2904–2910. [PubMed: 16799032]
8. Sadun AA, Carelli V, Bose S, et al. First Application of Extremely High Resolution Magnetic Resonance Imaging to Study Microscopic Features of Normal and LHON Human Optic Nerve. Ophthalmology 2002;109:1085–1091. [PubMed: 12045048]
9. Guo L, Tsatourian V, Luong V, et al. En face optical coherence tomography: a new method to analyse structural changes of the optic nerve head in rat glaucoma. British Journal of Ophthalmology 2005:1–7. [PubMed: 15615733]
10. Barkana Y, Harizman N, Gerber Y, Liebmann JM, Ritch R. Measurements of optic disk size with HRT II, Stratus OCT, and funduscopy are not interchangeable. Am J Ophthalmol 2006;142:375–380. [PubMed: 16935579]
11. Boyer KL, Herzog A, Roberts C. Automatic recovery of the optic nervehead geometry in optical coherence tomography. IEEE Trans Med Imaging 2006;25:553–570. [PubMed: 16689260]
12. Wojtkowski M, Srinivasan V, Fujimoto JG, et al. Three-dimensional retinal imaging with high-speed ultrahigh-resolution optical coherence tomography. Ophthalmology 2005;112:1734–1746. [PubMed: 16140383]

13. Ramakrishnan R, Kader MA, Budde WM. Optic disc morphometry with optical coherence tomography: comparison with planimetry of fundus photographs and influence of parapapillary atrophy and pigmentary conus. Indian J Ophthalmol 2005;53:187–191. [PubMed: 16137964]
14. Floyd MS, Katz BJ, Digre KB. Measurement of the scleral canal using optical coherence tomography in patients with optic nerve drusen. Am J Ophthalmol 2005;139:664–669. [PubMed: 15808162]
15. Wojtkowski M, Bajraszewski T, Gorczynska I, et al. Ophthalmic imaging by spectral optical coherence tomography. Am J Ophthalmol 2004;138:412–419. [PubMed: 15364223]
16. Lai E, Wollstein G, Price LL, et al. Optical coherence tomography disc assessment in optic nerves with peripapillary atrophy. Ophthalmic Surg Lasers Imaging 2003;34:498–504. [PubMed: 14620759]
17. Bellezza AJ, Hart RT, Burgoyne CF. The optic nerve head as a biomechanical structure: initial finite element modeling. Invest Ophthalmol Vis Sci 2000;41:2991–3000. [PubMed: 10967056]
18. Sigal IA, Flanagan JG, Ethier CR. Factors influencing optic nerve head biomechanics. Invest Ophthalmol Vis Sci 2005;46:4189–4199. [PubMed: 16249498]
19. Sigal IA, Flanagan JG, Tertinegg I, Ethier CR. Reconstruction of human optic nerve heads for finite element modeling. Technol Health Care 2005;13:313–329. [PubMed: 16055979]
20. Sigal IA, Flanagan JG, Tertinegg I, Ethier CR. Finite element modeling of optic nerve head biomechanics. Invest Ophthalmol Vis Sci 2004;45:4378–4387. [PubMed: 15557446]
21. Heickell AG, Bellezza AJ, Thompson HW, Burgoyne CF. Optic disc surface compliance testing using confocal scanning laser tomography in the normal monkey eye. J Glaucoma 2001;10:369–382. [PubMed: 11711833]
22. Burgoyne CF, Quigley HA, Thompson HW, Vitale S, Varma R. Early changes in optic disc compliance and surface position in experimental glaucoma. Ophthalmology 1995;102:1800–1809. [PubMed: 9098280]
23. Burgoyne CF, Morrison JC. The Anatomy and Pathophysiology of the Optic Nerve Head in Glaucoma. Journal of Glaucoma 2001;10:S16–S18. [PubMed: 11890263]
24. Yablonski M, Asamoto A. Basic sciences in clinical glaucoma: Hypothesis concerning the pathophysiology of optic nerve damage in open angle glaucoma. j Glaucoma 1993;2:119–127.
25. Emery JM, Landis D, Paton D, Boniuk M, Craig JM. The lamina cribrosa in normal and glaucomatous human eyes. Trans Am Acad Ophthalmol Otolaryngol 1974;78:OP290–297. [PubMed: 4825057]
26. Quigley HA, Hohman RM, Addicks EM, Massof RW, Green WR. Morphologic changes in the lamina cribrosa correlated with neural loss in open-angle glaucoma. Am J Ophthalmol 1983;95:673–691. [PubMed: 6846459]
27. Yan DB, Coloma FM, Metheetrairut A, et al. Deformation of the lamina cribrosa by elevated intraocular pressure. Br J Ophthalmol 1994;78:643–648. [PubMed: 7918293]
28. Quigley HA, Addicks EM, Green WR. Optic nerve damage in human glaucoma. III. Quantitative correlation of nerve fiber loss and visual field defect in glaucoma, ischemic neuropathy, papilledema, and toxic neuropathy. Arch Ophthalmol 1982;100:135–146. [PubMed: 7055464]
29. Quigley HA, Green WR. The histology of human glaucoma cupping and optic nerve damage: clinicopathologic correlation in 21 eyes. Ophthalmology 1979;86:1803–1830. [PubMed: 553256]

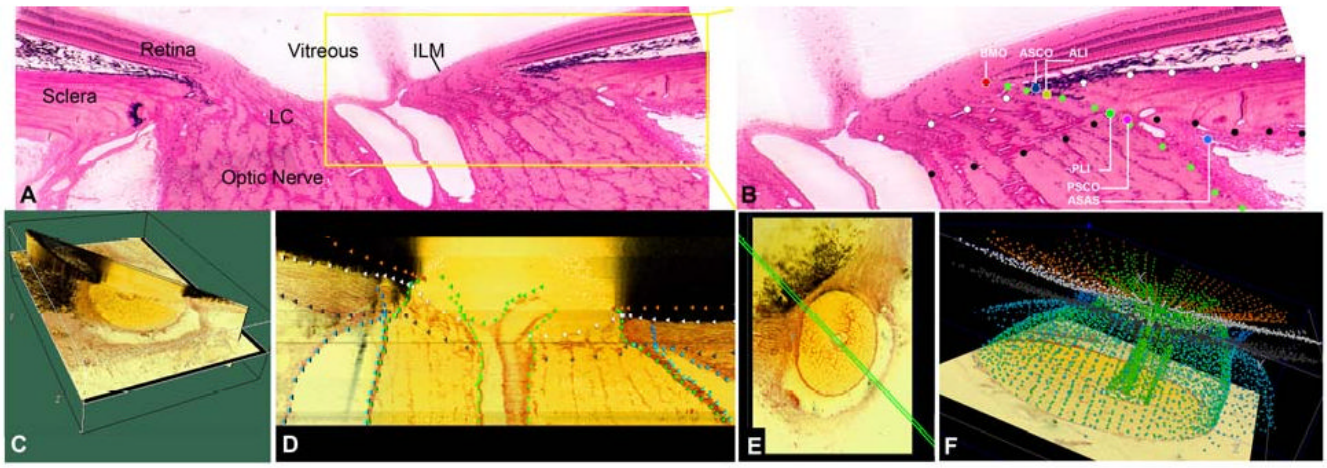

Figure 1. 3D delineation of ONH and peripapillary scleral landmark points within colorized, stacked-section, 3D ONH reconstructions

Note that generation of 3D ONH reconstruction from aligned serial section images for each individual ONH are explained in Figures 1 and 2 of our previous publication[2]. **A.** Sagittal histologic section through a representative normal monkey ONH showing the anatomy, and (**B**) the associated neural canal landmarks and surface landmarks: Bruch's membrane opening (BMO, red), the anterior scleral canal opening (ASCO, dark blue), the anterior laminar insertion point (ALI, yellow), the posterior laminar insertion point (PLI, green), the posterior scleral canal opening (PSCO, pink), the anterior-most aspect of the subarachnoid space (ASAS, light blue), the anterior laminar/scleral surface (white), the posterior laminar/scleral surface (black) and the neural boundary (light green). **C.** A total of 40 serial digital, radial, sagittal slices (seen in D, each 7 voxels thick) are served to the delineator at 4.5° intervals. **D.** A representative digital sagittal slice, showing the marks for 7 landmark surfaces and 6 pairs of landmark points, which are 3D-delineated using linked, simultaneous, co-localization of the sagittal slice (shown) and the transverse section image[4] (**E**). **F.** Representative 3D point cloud showing all delineated points for a normal monkey ONH relative to the last serial section image (orbital optic nerve bottom, vitreous above.

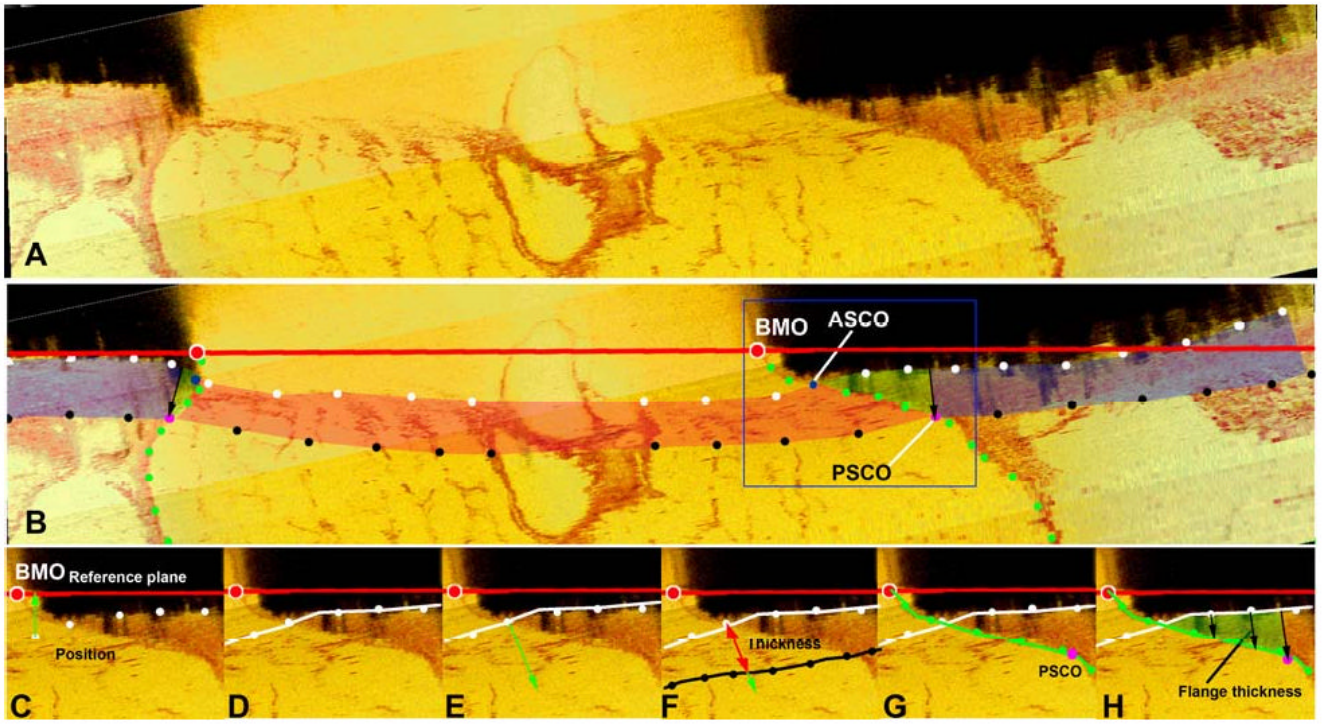

Figure 2. ONH anatomy and parameter generation

A) Representative horizontal, digital sagittal section image from the 3D reconstruction of the left eye of Monkey 3 (temporal on left, nasal on right). **B**) The definition and extent of the major structures quantified in the paper: lamina cribrosa (red) inserts into the scleral flange (green), which transitions into the peripapillary sclera (purple) at the PSCO. The delineated points marking the anterior (white dots) and posterior (black dots) surfaces of the lamina cribrosa and sclera, the neural canal boundary (green dots), and neural canal landmark points are shown. The scleral flange is defined as the peripapillary sclera that extends from the anterior scleral canal opening (ASCO) to the normal from the anterior surface through the posterior scleral canal opening (PSCO normal vector - black arrow). The Bruch's Membrane opening (BMO) zero reference plane is also shown (red line). **C**) Laminar and scleral position (green arrow) at each delineated anterior laminar surface point (white dot) is defined as the shortest distance from the delineated point to BMO zero reference plane. **D**) LC and PPS thickness at each delineated anterior surface point is determined by fitting a continuous surface (white line) to all of the delineated anterior surface points (**D**). **E, F**) Thickness is defined as the distance along a normal vector to the anterior surface (green arrow in **E**) from each anterior delineated point to the posterior surface (black line in **F**). **G**) Thickness of the scleral flange at each delineated anterior surface point (white dots) is defined as the distance between the neural canal boundary points (green line in **G** and **H**), along a vector parallel to the PSCO normal vector.

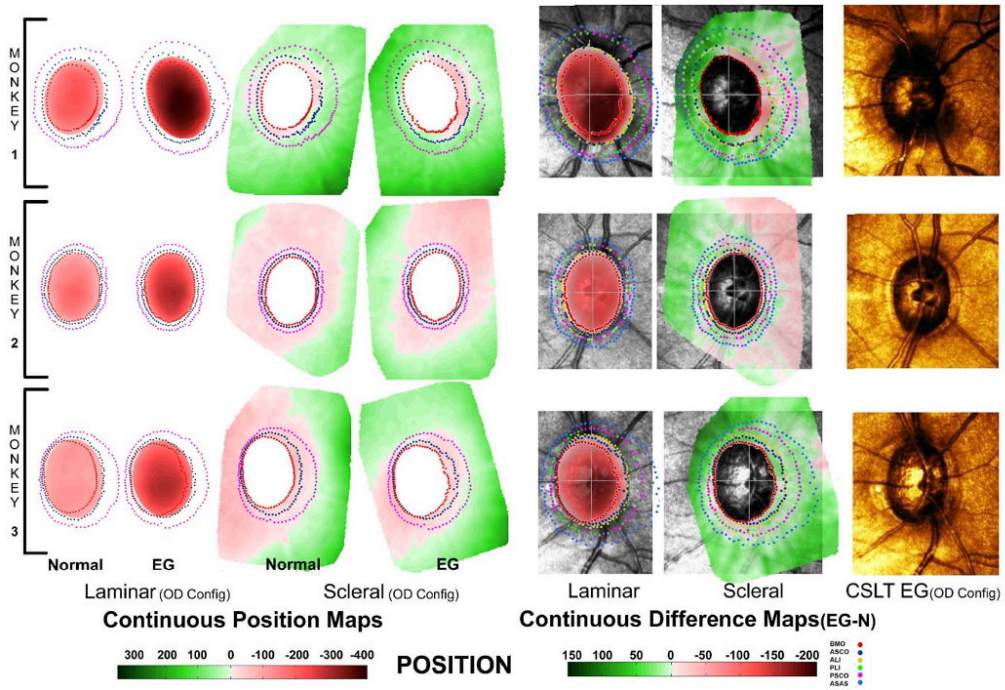

Figure 3. Continuous lamina cribrosa and peripapillary scleral position (μm) maps for both eyes and continuous treatment difference maps for each monkey co-localized with neural canal landmark points[4]

Continuous laminar position maps of the Normal and EG eye of each monkey (**2 left columns**; both in right eye configuration) overlaid with a subset of neural canal landmark points for reference. Continuous scleral flange and peripapillary scleral position maps of Normal and EG eye (**3rd and 4th columns**; both in right eye configuration). Continuous treatment difference maps (EG eye data – Normal eye data) for laminar, scleral flange, and peripapillary scleral position (**5th and 6th columns**) overlaid onto the CSLT image of the EG eye. CSLT images of EG eye of each monkey (**far right column** in right eye configuration) for reference.

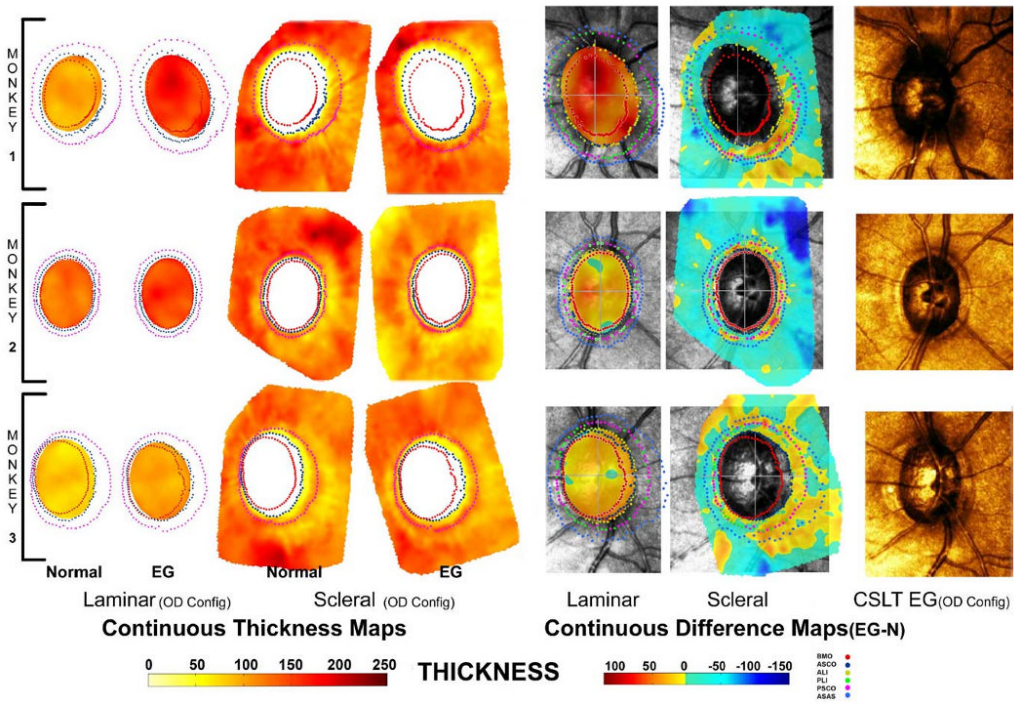

Figure 4. Continuous lamina cribrosa and peripapillary scleral thickness (μm) maps for both eyes and continuous treatment difference maps for each monkey co-localized with neural canal landmark points[4]

Continuous laminar thickness maps of the Normal and EG eye of each monkey (**2 left columns**; both in right eye configuration) overlaid with a subset of neural canal landmark points for reference. Continuous scleral flange and peripapillary scleral thickness maps of Normal and EG eye (**3rd and 4th columns**; both in right eye configuration). Continuous treatment difference maps (EG eye data – Normal eye data) for laminar, scleral flange, and peripapillary scleral thickness (**5th and 6th columns**) overlaid onto the CSLT image of the EG eye. CSLT images of EG eye of each monkey (**far right column** in right eye configuration) for reference.

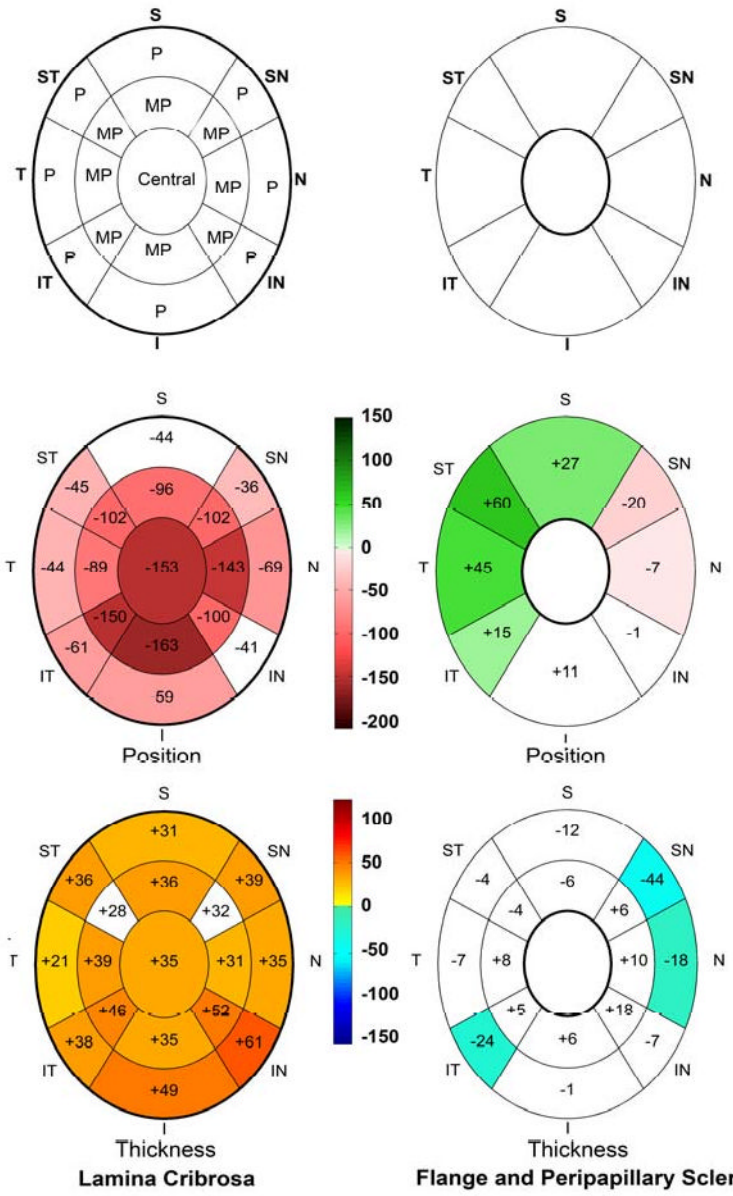

Figure 5. Regionalization method and overall regional position and thickness treatment differences (EG-N) within the lamina cribrosa, scleral flange, and peripapillary sclera

Within the lamina, position and thickness data are pooled into 17 regions according to the three radial regions (central; MP, middle periphery; P, periphery) and eight quadrants (S, superior; SN, supero-nasal; N, nasal; IN, infero-nasal; I, inferior; IT, infero-temporal; T, temporal; ST, supero-temporal) (**top left**). Scleral flange and peripapillary sclera data, together, are pooled into 8 quadrants (**top right**). Overall laminar position treatment difference (**middle left**) and pooled peripapillary scleral position treatment difference (**middle right**). Regional thickness difference in the lamina cribrosa (**bottom left**), scleral flange (**bottom right** inner ring), and peripapillary sclera (**bottom right** outer ring). Values shown (in μm) are the magnitude of change in the EG eye relative to its contralateral Normal control (EG-N). The colored regions achieved statistically significant difference between the normal and EG eyes ($P<0.05$, ANOVA). Color intensity represents magnitude as illustrated in the color bar. For position data, red indicates posterior deformation and green indicates anterior deformation in the EG

eyes relative to their contralateral Normal controls. For thickness data, yellow to red indicates an increase in thickness and green to blue indicates a decrease in thickness in the EG eyes relative to their contralateral Normal controls.

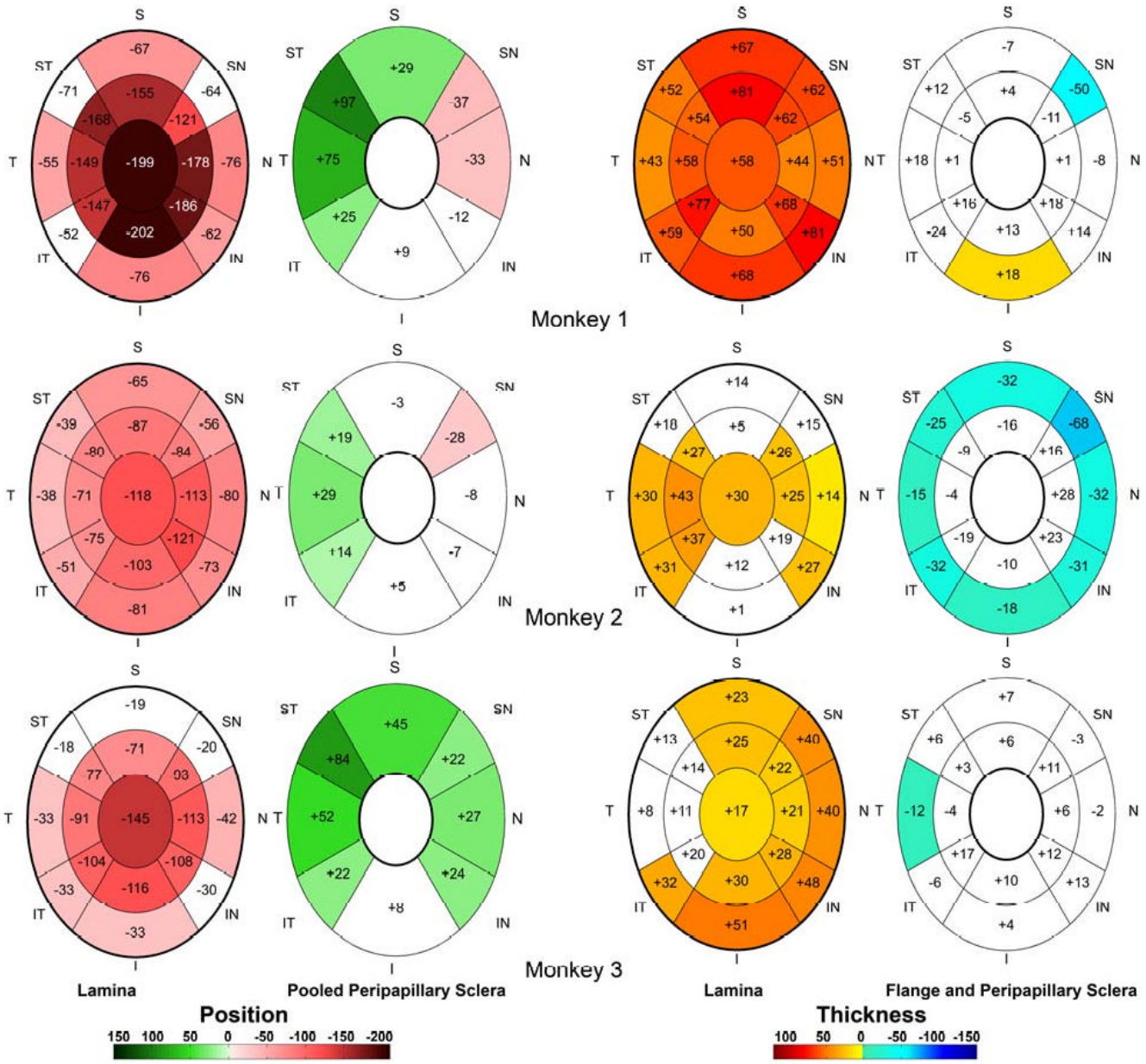

Figure 6. Regional treatment differences in position (μm) and thickness (μm) of the lamina cribrosa, scleral flange, and peripapillary sclera by monkey (Delineator 1 (JCD) data)

The colored regions indicate statistically significant differences between Normal and EG eyes (P<0.05, ANOVA). Color intensity represents the magnitude of difference as illustrated in the color bars. For the position data, red indicates posterior deformation and green indicates anterior deformation in the EG eyes compared to their contralateral Normal controls. For the thickness data, yellow to red indicates an increase in thickness and green to blue indicates a decrease in thickness in the EG eyes compared to their contralateral Normal controls.

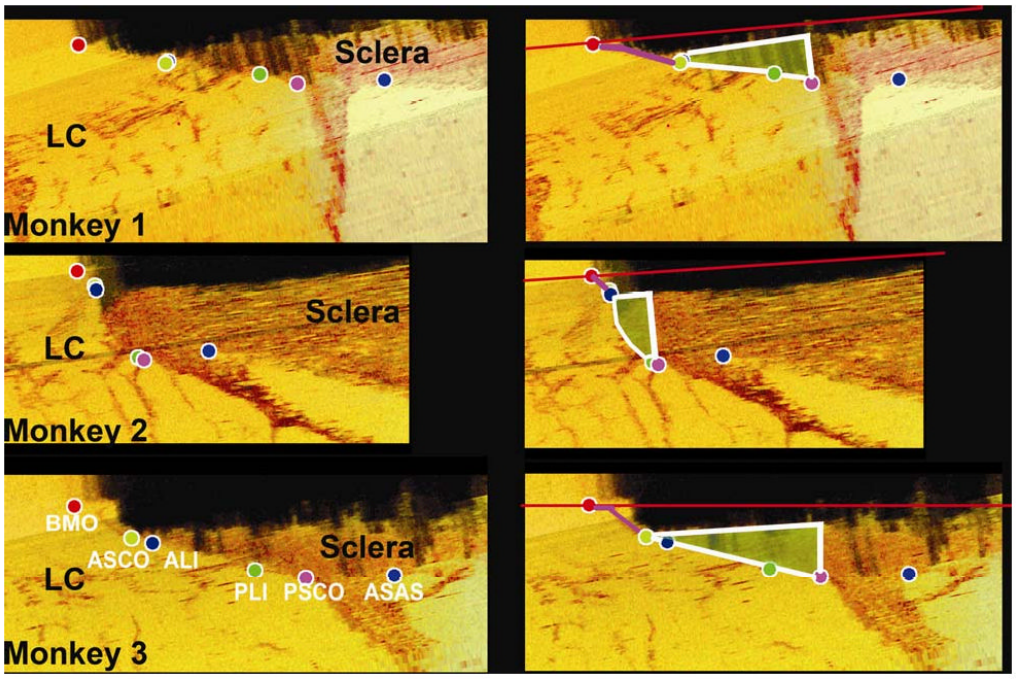

Figure 7. Neural canal landmarks and scleral flange architecture within the nasal region of the Normal eye of each monkey

Neural canal landmarks within a digital sagittal section of the nasal ONH for each Normal eye (**left**). Border Tissues of Elschnig (purple) and scleral flange (green) (**right**); note the relationship between regional neural canal obliqueness and scleral flange obliqueness in each eye. In general, a more oblique neural canal results in a more oblique scleral flange. While regional neural canal and scleral flange obliqueness are related, they may have separate clinical implications. The clinical importance of these anatomic features remains to be determined.

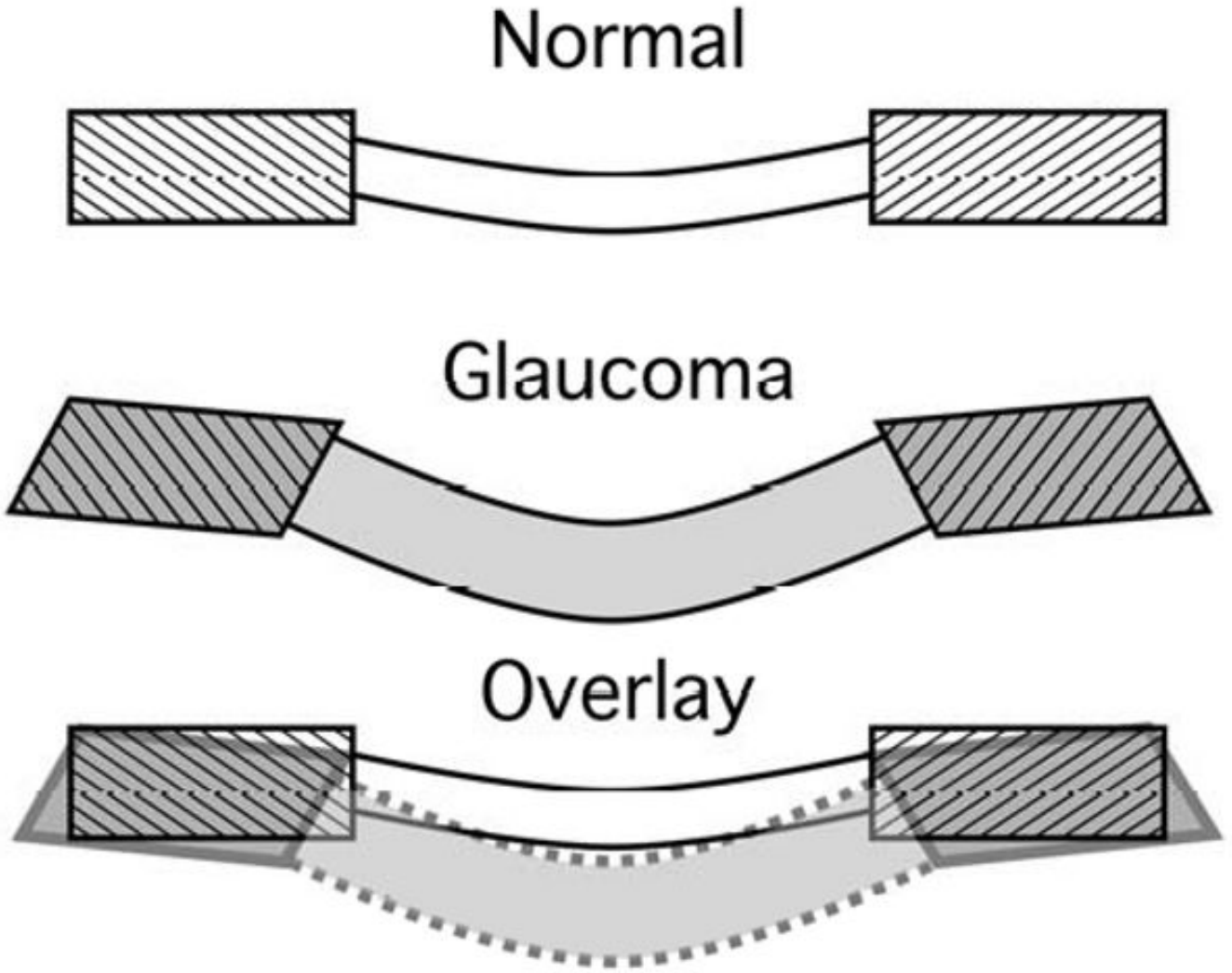

Figure 8. Schematic diagram of the macro-scale connective tissue architecture in the Normal and EG monkey eye

Normal lamina cribrosa, scleral flange and peripapillary position and thickness are schematically represented in the upper illustration. In EG (**middle**), the lamina cribrosa is thickened and posteriorly deformed, greatest centrally, with focal progression to the periphery (not shown). The scleral flange and peripapillary sclera are together displaced posteriorly, with most of the displacement in the sclera occurring closest to the neural canal. The posterior aspect of the neural canal is diffusely expanded in EG[4], while the anterior entrance to the neural canal is only focally expanded (not shown). Diagrams of Normal (black) and EG (grey) ONH architecture are overlaid in the bottom illustration.

Table 1

Position and thickness of lamina cribrosa, scleral flange, and peripapillary sclera

Overall results by delineator (note treatment values, ΔEG, are the EG eye measure - the N eye measure).

	Delineator 1		Delineator 2		Delineator 3		Delineator 4		Delineator 5	
Structure	**N**	**ΔEG**	**N**	**ΔEG**	**N**	**ΔEG**	**N**	**ΔEG**	**N**	**ΔEG**
Laminar Position	-106	**-99***	-94	**-90***	-98	**-97***	-94	**-106***	-88	**-91***
PP Sclera Position	-4	**16***	19	**16***	17	**33***	7	**44***	6	**38***
Laminar Thickness	105	**38***	111	**62***	118	**56***	121	**49***	105	**30***
Flange Thickness	69	7	64	**11***	72	**9***	66	**21***	58	15
Peripapillary Scleral Thickness	123	**-14***	126	**21***	132	-1	143	1	105	**-9***

*$P<0.05$, ANOVA

Table 2

Position and thickness of lamina cribrosa, scleral flange, and peripapillary sclera

Overall results by monkey (note treatment values, ΔEG, are the EG eye measure - the N eye measure).

Structure	Monkey 1		Monkey 2		Monkey 3	
	N	ΔEG	N	ΔEG	N	ΔEG
Laminar Position	-102	**-118***	-111	**-97***	-105	**-79***
PP Sclera Position	45	**21***	-14	3	-37	**35***
Laminar Thickness	103	**61***	128	**23***	83	**26***
Flange Thickness	69	7	76	1	60	8
Peripapillary Scleral Thickness	136	-4	126	**-32***	113	1

*$P<0.05$, ANOVA

Table 3

Position and thickness of lamina cribrosa, scleral flange, and peripapillary sclera

Overall results by delineator and day (note treatment values, ΔEG, are the EG eye measure - the N eye measure).

	Delineator 3						Delineator 4					
Structure	**N Day 1**	**N Day 2**	**N Day 3**	**ΔEG Day 1**	**ΔEG Day 2**	**ΔEG Day 3**	**N Day 1**	**N Day 2**	**N Day 3**	**ΔEG Day 1**	**ΔEG Day 2**	**ΔEG Day 3**
Laminar Position	-106	-106	-103	**-96***	**-97***	**-94***	-102	-101	-100	**-97***	**-98***	**-98***
PP Sclera Position	-38	-34	-31	**50***	**43***	**43***	-47	-43	-39	**39***	**40***	**47***
Laminar Thickness	92	117	118	**40***	**5***	**8***	102	88	87	**17***	**14***	**21***
Flange Thickness	61	55	67	4	9	-1	40	50	51	**31***	**14***	13
Peripapillary Scleral Thickness	111	112	116	**-8***	**-7***	**-7***	102	112	110	**12***	0	0

*$P<0.05$, ANOVA